International Journal of Emerging Science and Engineering (IJESE)
ISSN: 2319–6378 (Online), Volume-12 Issue-6, May 2024

A Case Study on Image Co-Registration of Hyper-Spectral and Dual (L & S) Band SAR Data and Ore Findings Over Zewar Mines, India

Dipanjan Dutta, Tamesh Halder, Abhishek Penchala, Kandukoori Vamshi Krishna, Grajula Prashnath, Debashish Chakravarty

Abstract: ***The technique of superimposing two or more photographs in a way that ensures that for each image, the same pixel corresponds to the same location of the target scene is known as image coregistration It is a crucial stage in the picture enhancement process for satellite images. Different frequency bands store feature. Image fusion makes it possible to superimpose co-registered pictures taken by several sensors to get a superior image incorporating elements from both sources. On many match patches that are evenly dispersed over the two scenes, we estimate pixel offsets between possibly coherent picture pairings as image coregistration allows a more detailed single image to be obtained than many photos with distinct attributes. This study presents existing various fusion methods for ASAR (Airborne Synthetic Aperture Radar) images in the S-band and L-band to interpret urban, forestry, and agricultural areas. AVIRIS hyper spectral data also shows mining possibilities on ore of region. Hence, the seeking of ore region, and coregistration using fusion facilitates the remote sensing architecture next to drones.***

Keywords: Co-registration, AVIRIS, Fusion, ASAR, S-Band, L-Band.

I. INTRODUCTION

The technique of matching two or more images in such a way that each pixel corresponds to the same place in the target scene is known as image coregistration. Numerous remote sensing tasks, including multi-sensor categorization, change detection, mosaicking, synthetic aperture radar (SAR) interferometry, radargrammetry, photogrammetry, and multi-sensor data fusion, can benefit from this method.

Manuscript received on 12 April 2024 | Revised Manuscript received on 18 April 2024 | Manuscript Accepted on 15 May 2024 | Manuscript published on 30 May 2024.

***Correspondence Author(s)**

Dipanjan Dutta, Department of Electronics, KIIT, Bhuwenswar, Odhisa, India. E-mail: Dipanjandutta121@gmail.com

Tamesh Halder*, Department of Mining Engineering, IIT Kharagpur, Kharagpur (West Bengal), India. E-mail: haldertamesh@iitkgp.ac.in, ORCID ID: 0000-0002-9363-1471

Abhishek Penchala, Department of Mining Engineering, IIT Kharagpur (West Bengal), India. E-mail: haldertamesh@gmail.com, ORCID ID: 0009-0007-9820-1933

Kandukoori Vamshi Krishna, Department of Mining Engineerin, Zewar Mines, Zewar (Rajasthan), India. Email: Kandukurivamshikrishna@gmail.com

Grajula Prashnath, Department of Mining Engineering. Zewar Mines, Zewar (Rajasthan), India. E-mail: prashanthgajula59@gmail.com

Debashish Chakravarty, Department of Mining Engineering, IIT Khragpur (West Bengal), India. E-mail: profdciitkgp@gmail.com

It is a crucial step in remote sensing to ensure accurate and coherent analysis of the captured data from different sensors or times [1] [23] [24]. In remote sensing, Panchromatic and multispectral photos of the exact location are provided separately by airborne satellites. A crucial step in image processing is registration, which is used to compare two or more pictures that were taken from various angles, sensors, or times. The choice of coregistration technique depends on the specific application, such as change detection, interferometry, or fusion.

The coregistration procedure entails several steps, including coarse coregistration with up to 1- or 2-pixel accuracy using a common spatial sample, fine coregistration to find the remaining transformation, fitting transformation equations, and resampling the slave image based on subpixel transformations [2]. Various suggested algorithms employ various ways to find and assess picture similarity. Feature-based approaches try to identify ground objects based on discrete identification traits that are consistent throughout time and location, such as crossroads, buildings, agricultural parcel margins, or strongly defined mountain ridges. Due to the rising volume of remote sensing data and the requirement for completely automated pipelines that exploit multi-sensoral and multi-temporal data, efficient and rapid image co-registration approaches are needed [3]. The ultimate objective is to develop a robust algorithm capable of handling the heterogeneity of globally gathered satellite data from various sensors, air conditions, collection times, and illumination geometries. This study presents a general and automated co-registration technique for georeferenced satellite pictures, achieving sub-pixel accuracy. A multimodal image coregistration approach is described in this paper, which incorporates two fundamental concepts: using complimentary geometry information between the pictures to be coregistered and using mutual information (or entropy) as a similarity measure. These methods successfully handle issues caused by variances in radiometries and geometries [4]. The approach is primarily intended for coregistration of high-resolution synthetic aperture radar (SAR) and optical pictures, although it is also applicable in other situations. The method's efficiency has been verified by tests on actual, extremely high-resolution optical and SAR data, demonstrating its potential for precise and dependable image coregistration.

II. METHODOLOGY

We used ASAR data of Dewalt, Zawar Mines, Rajasthan in the S-band and L-band frequency channels from ISRO. The S-band and L-band data were processed separately to provide 3-channel images of the location.

1. S-band has a frequency range of 2 to 4 GHz, straddling the usual border between UHF and SHF at 3 GHz. The plant cover in canopies is greater in the S-band.
2. L-band operates between 1 and 2 GHz. Signals sent in the L-band exhibit the second-lowest loss and may pass through foliage and dense cover. Offers a more precise picture than other bands under cloudy weather. Low backscatter characterises L-band. L-Band has the benefit of less rain fading interference, cheaper equipment, smaller antennas, and S-Band is less sensitive to rain fading when compared to Ku and Ka bands. Broader bandwidths are frequently accessible in higher frequency bands. However, they are also more susceptible to "rain fade," which is the atmospheric absorption of radio signals by rain, snow, or ice.As L-band has lowest frequency we can observe that it can pass through foliage and dense cover forest, whereas S-band has larger frequency it doesn't pass through foliage and dense cover, it got stuck to the upper surface of the forest(Figure1).

Figure 1. L-band and S-band Effects

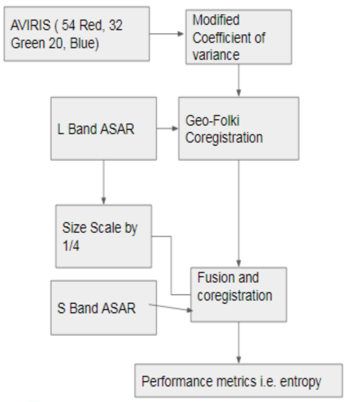

Figure 2. Methodology Workflow

- Date of data:
  ASAR FP: 28/06 2017
  AVIRIS: 02/02/2016

We have applied various types of diffusion techniques for analyzing our desired output. We have done coregistration process with Aviris data with Lband full polarized SAR data as a result we have obtained the modified coefficient of variance of AVIRIS in Red band and it is registered with the L band ASAR data using GeoFolki algorithm. L band and S band ASAR fused data is combined with AVIRIS process data. The L band data first scale down by 2 in range and azimuth. The L band ASAR data diffused with the S-band by using following methods:-

1. ADF [5, 18, 19]:- anisotropy diffusion fusion is used to divide the source images into detail and approximation layers. Karhunen-Loeve transformation and the final approximation and detail layers are computed via weighted linear superposition. The final detail and approximation layers are blended into a single image.

2. CBF [6]:-The bilateral cross filter extracts detailed pictures from the source photos for weight computation. These weights, determined by evaluating the degree to which horizontal and vertical features are present, are applied directly to the source photos.

3. CNN [7]:- The merging approach takes into account the unique imaging modalities of infrared and visible images and fuses them at numerous scales utilising picture pyramids. The fusion mode is then dynamically adjusted for the decomposed coefficients using a local similarity-based technique, ensuring flexibility during the fusion process.

4. HMSD_GF [8]:- In hybrid multi-scale decomposition by guided filter the infrared image data is merged with the visible picture using a multi-scale fusion approach based on a hybrid multi-scale decomposition by guided filter. Moreover, a perceptual-based regularization parameter selection technique is applied to analyze the relative contribution of infrared spectral features by comparing the perceptual saliency of both infrared and visible image information.

5. IFEVIP [9]: In Infrared Feature Extraction and Visual Information Preservation, the process begins with the use of Bézier interpolation and quadtree decomposition to reconstruct the 1st picture backdrop. Next, the bright features are extracted by subtracting the reconstructed backdrop from the original 1st image, effectively eliminating unnecessary background information. To avoid overexposure, the enhanced 1st image features are selectively attenuated before being combined with the visible picture to create the final fusion image.

6. MGFF [10]:-In Multiscale guided filter, Multi-scale image decomposition is useful for representing and manipulating picture characteristics at different sizes. By transferring structures, this technique is able to insert structures from one source image into another. This paper provides a unique visual saliency detection method based on guided image filters that might be useful in locating significant regions in visually different pictures of the same scene. The use of weight maps allowed the supplemental data to be integrated pixel-by-pixel at each scale.

7. TIF [11] [27]:- In Two-scale image fusion, the invention of a unique weight map generating technique based on visual saliency is recommended. With this method, the combined image might include artistically important details from the original photos. The suggested strategy solely employs two-scale picture decomposition, unlike the majority of multi-scale image fusion methods. Thus, it is quick and effective.

8, DWT [20]:- With introducing discrete wavelet transform, so a lowpass mean equaliser to the required areas containing the items, we create two pictures with variously blurred objects.

Published By:
Blue Eyes Intelligence Engineering and Sciences Publication (BEIESP)

The results presented in this section were acquired using two input photos even though we have utilised more than two images. We contrast several merging techniques, various degrees of resolution, and various wavelet families. We utilise an objective criteria as a quality indicator which is RMSE.

9. **PCA [21]:** The multispectral bands are subject to the Principal Component Analysis . The first PCA's histogram is matched to the panchromatic picture. The chosen component is then replaced, and the fused dataset is then transformed using an inverse PCA to return it to the initial multispectral feature space. The benefit of PC fusion is that there are no restrictions on the number of bands, but because it is a statistical method, it is vulnerable to the region that has to be sharpened and generates fusion results that might vary based on the chosen picture subsets.

10. **IHS [21] [25] [26]:** A collection of calculations make up the Brovey transform or Intensity Hue Saturation. The total of the three selected bands is divided by each spectral band and then multiplied by a picture that is monochromatic.

III. EVALUATION METRICS

AVIRIS has results on modified coefficient of variance(mean*median/variance). We took Red band. There have been several evaluation methods proposed for optical-SAR image fusion. Human perception-based metrics, metrics based on human perception, and metrics based on similarity of picture structure may be divided, as stated in [12][13]. But none of the suggested measures is superior to the others. We incorporated 6 assessment measures in VIFB to enable a thorough and impartial performance comparison. All these measures can be easily calculated for any method in VIFB, which makes comparing method performances simple [14-17].

IV. RESULTS

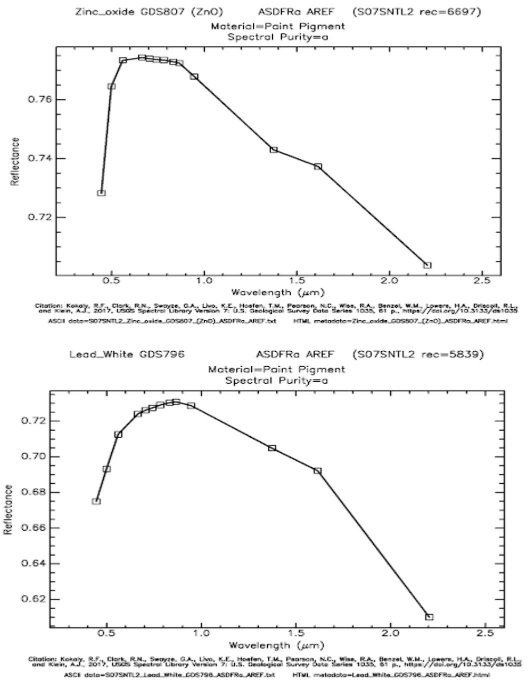

Figure 3. Zinc Oxide and Led Oxide Optimal Band Selection

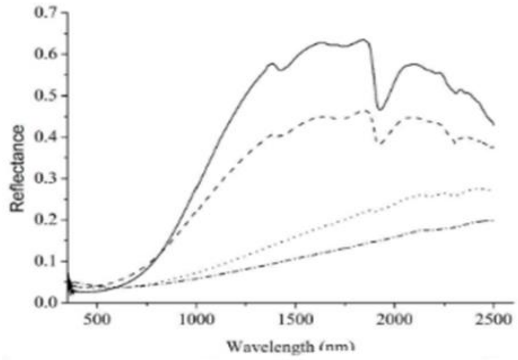

Figure 4. Coal Reflection Properties vs Wavelength [22]

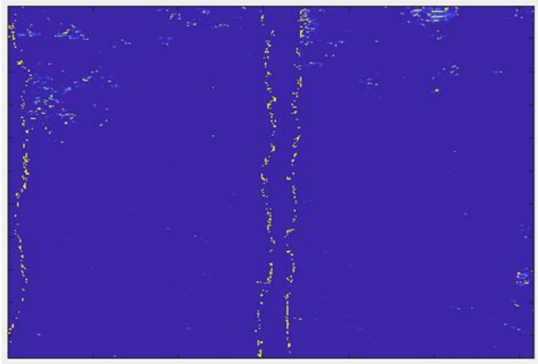

Figure 5: AVIRIS Modified Coefficient of Variance

Figure 6: Scaled L band Image

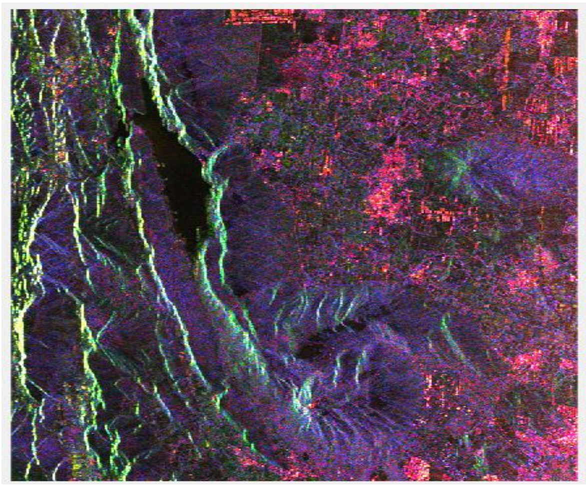

Figure 7: L-Band Image

Retrieval Number: 100.1/ijese.A805513010524
DOI: 10.35940/ijese.A8055.12060524
Journal Website: www.ijese.org

Published By:
Blue Eyes Intelligence Engineering
and Sciences Publication (BEIESP)

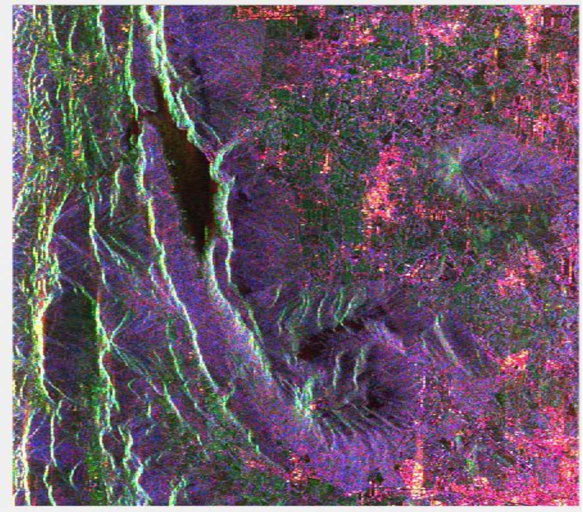

Figure 8: S Band Image

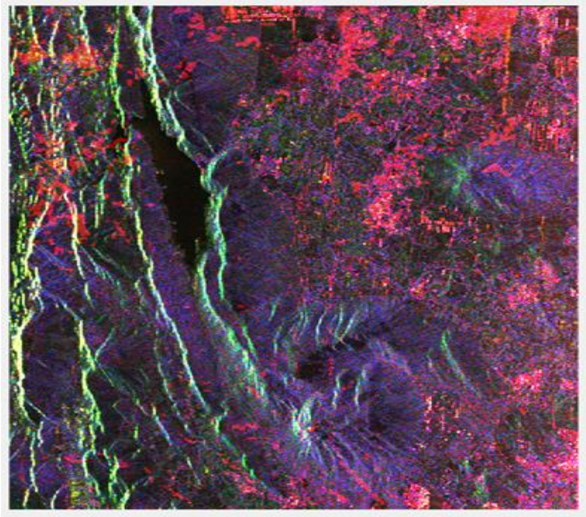

Figure 11: Fused image by CNN

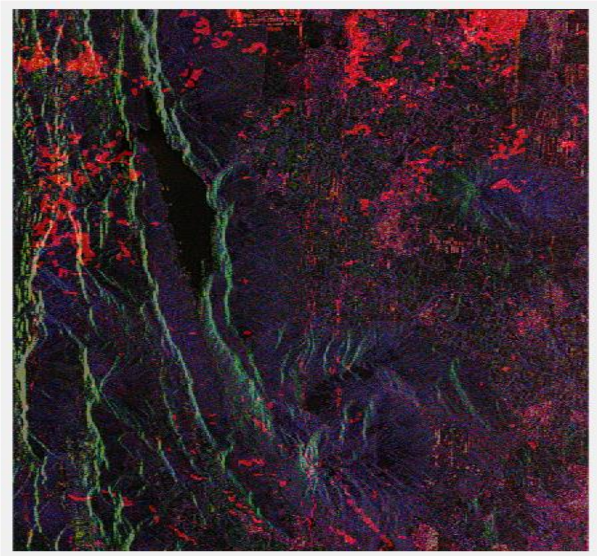

Figure 9: Fusion Image by ADF

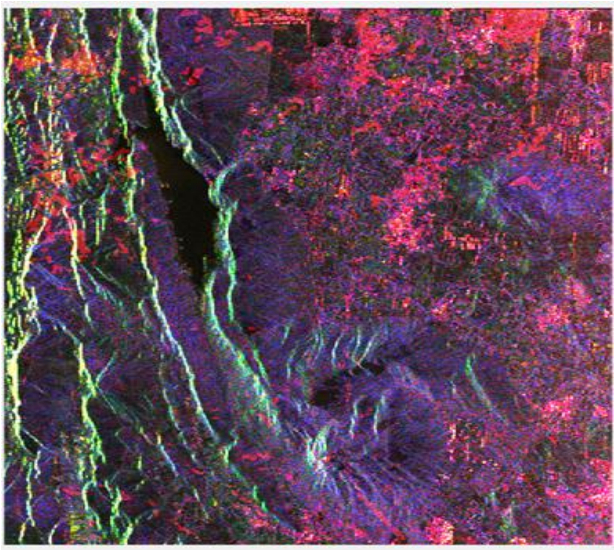

Figure 12: Fused Image by HMSD-GF

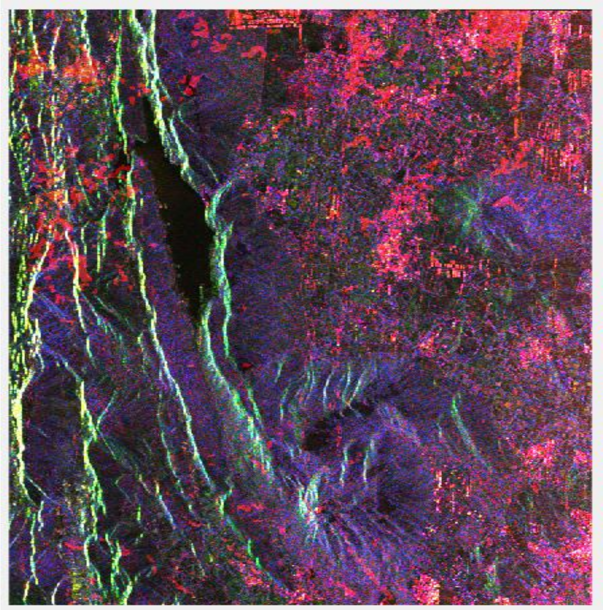

Figure 10: Fusion Image by CBF

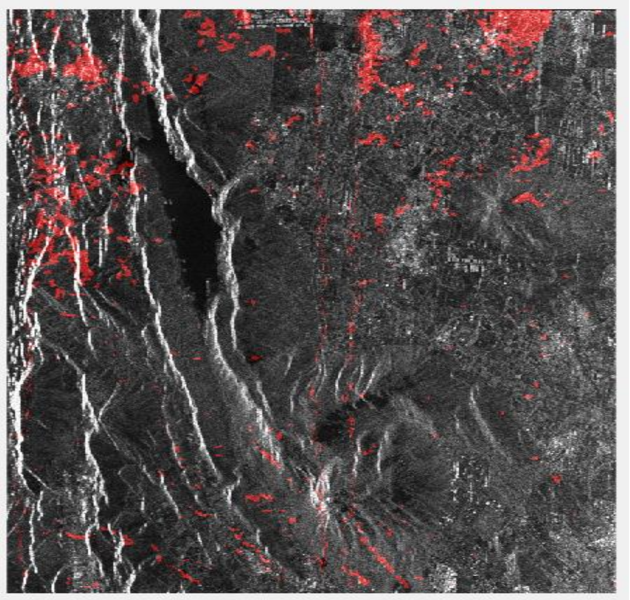

Figure 13: Image Fusion by IFEVIP

Retrieval Number: 100.1/ijese.A805513010524
DOI: [10.35940/ijese.A8055.12060524](https://doi.org/10.35940/ijese.A8055.12060524)
Journal Website: www.ijese.org

Published By:
Blue Eyes Intelligence Engineering
and Sciences Publication (BEIESP)

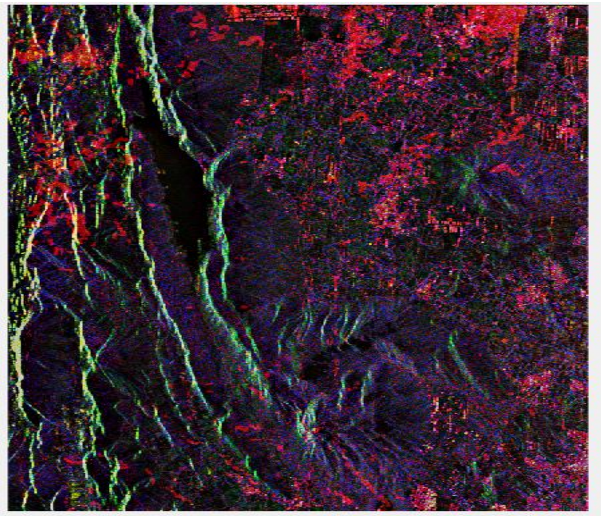

Figure 14: Image Fusion by MGFF

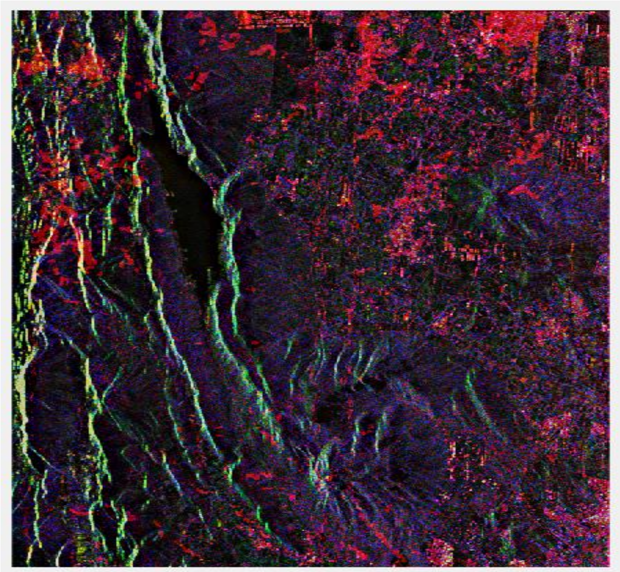

Figure 15: Image Fusion by TIF

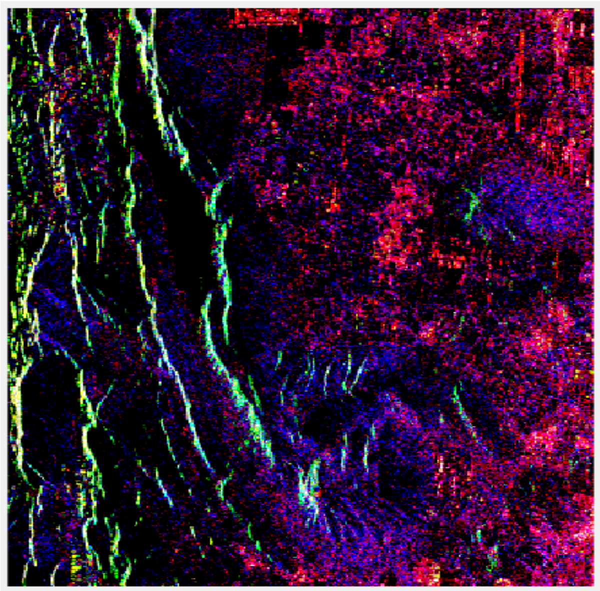

Figure 16: Image Fusion by DWT

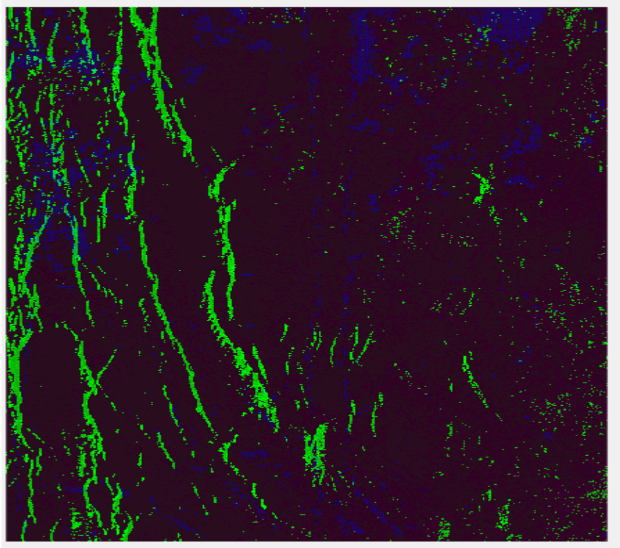

Figure 17: Image Fusion by PCA

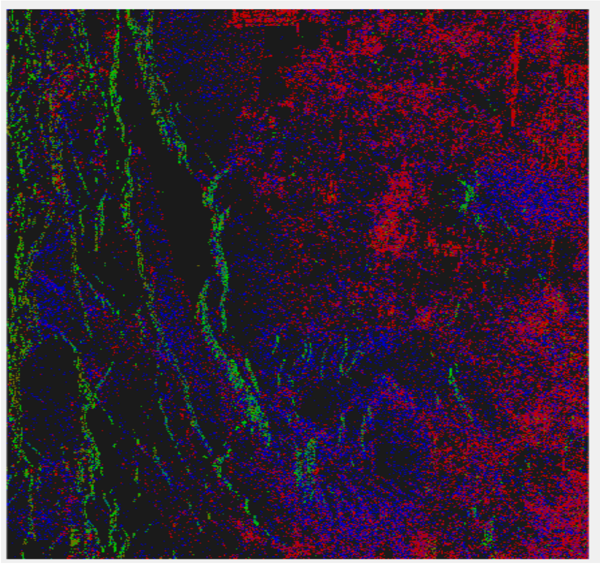

Figure 18: Image Fusion by HIS

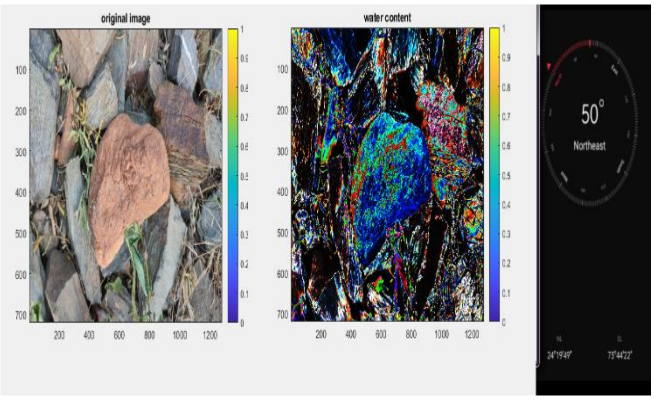

Figure 19. Ground truth of Zewar mines (Zinc blue and led red)

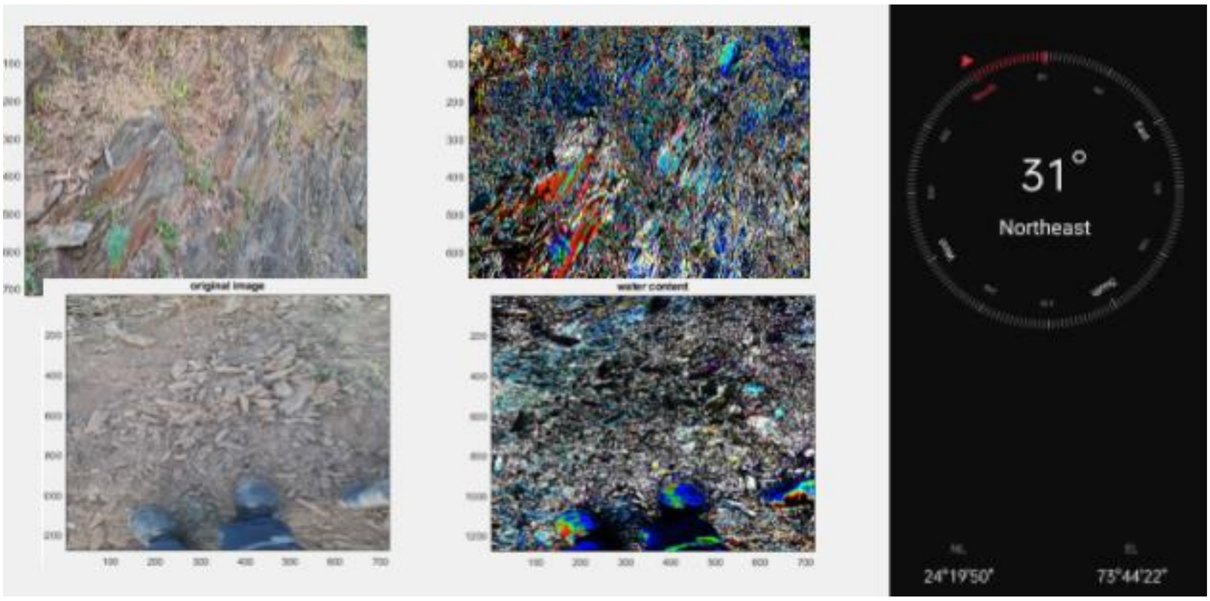

Figure 20: Ground Truth of Zewar Mines, India (Zinc Blue and Led Red)

Algorithm 1

```
geo_op=Geofolki(img1, AVIRIS);
fusion=MGFF (img1,img2)
img1(:,:,1)=im2uint8(fusion(:,:,1))+im2uint8(0.55*geo_op(:,:,1));axis off;
 img1(:,:,2:3)=fusion(:,:,2:3);
```

Table. 1 Performance Metrics of Fusion Based Coregistration Methods

Methods	AG	CE	EI	EN	MI	PSNR	QABP	QCB	QCV	RMSE	SF	SSM	SD
ADF	18.235	4.6041	152.67	5.2541	0.20967	54.854	0.07877	0.19178	1123.4	0.21319	64.549	0.13409	37.779
CBF	1.5803	4.9768	14.546	2.3128	0.060799	54.353	0.0086267	0.039918	1216.7	0.2388	10.237	0.070552	6.7729
CNN	1.5792	4.9745	14.534	2.3081	0.060808	54.353	0.0086225	0.039836	1216.7	0.2388	10.244	0.070501	6.7795
HMSD-GF	1.9221	5.9285	17.474	2.5143	0.065336	54.362	0.0099768	0.0454	1217.5	0.23832	12.735	0.071107	8.0168
IFEVIP	0.0072384	0.31404	0.053343	0.010979	0.0029567	54.297	0.0038626	0.011053	1227.8	0.24189	1.236	0.067353	0.74474
MGFF	28.965	2.2336	242.89	6.2705	0.30116	55.4	0.11225	0.34152	1499.7	0.18881	89.787	0.2096	62.048
TIF	15.848	1.8366	158.51	5.71	0.41696	57.963	0.12895	0.39452	1383.8	0.104	44.83	0.25533	55.024
DWT	15.8478	1.8366	158.5112	5.71	0.417	57.9632	O.1289	0.3945	1383.8	0.104	44.8305	0.2553	55.0239
PCA	5.2953	2.871	49.8009	4.8814	0.2236	57.933	0.0468	0.2994	1324.5	0.1051	25.1453	0.1287	22.5303
IHS	14.2193	1.447	128.4411	6.228	0.4237	58.3594	0.1233	0.4423	1090.8	0.095	43.2674	0.3795	34.4746

V. DISCUSSION

The optimised band selection criteria is fulfilled by Figure 3 and figure 4; hence RGB channels have been selected. Qualitative assessment techniques are essential for assessing the quality of fused pictures. These methods rely their judgments on the human visual system. Even though Deep Convolutional Neural Networks could be distinguished in final picture quality, our suggested fusion approach does not require training, which cuts down on training time and boosts efficiency. The MATLAB code for the fusion architecture works flawlessly and generates the combined image in less than a minute. Metrics used to gauge how well the merged image performs visually were inspired by human vision. The performance differences between qualitative and quantitative evaluations amply demonstrate the importance of qualitative and quantitative comparisons to assess the effectiveness of an image fusion. A powerful multichannel fusion approach for NISAR pictures is formed via an isotropic diffusion-based fusion method. The flow of fusion has the mean gradient and we measure this as an average gradient (AG). The cross-entropy (CE) depicts the fact that how similar and dissimilar from its entropy according to ergodicity. The edge intensity (EI) signifies the point spread function and the edge spread function was well demystified. Entropy (EN) tells how well sink source and bifurcation works. Which is generally found in [1/f or (1/f^2)] power curves. Mutual information (MI) shows how much difference we can find between two or more distributions. The peak signal to noise ratio (PSNR) shows the highest signal energy transfers from one image to another image. Hence the gamma variation, hue, and color can be understood.

Retrieval Number: 100.1/ijese.A805513010524
DOI: 10.35940/ijese.A8055.12060524
Journal Website: www.ijese.org

Published By:
Blue Eyes Intelligence Engineering and Sciences Publication (BEIESP)

Qabp is a performance metric that filters out the average intensity and direction of orientation. The sensitivity analysis can be done using Qcb. Local variance or projection-based saliency. Root mean square error (RMSE) is one of the popular methods for finding mismatched characteristics. Spatial frequency (SF) is the differential means to detrend the analysis of the presentable image. SSM Image quality assessment: from error visibility to structural similarity Lastly, the variance (SD) we can understand how much square distance from the mean of the Pearson regression line. The MGFF method works best. We also see Aviris[54 RED, 36 GREEN, 20 BLUE] has a modified coefficient of variances (mean*median/variance) that facilitates the mine ore spread over the region. The proposed fusion method is modification of a combination of MGFF and TIF where the AVRIS data is added with fusion of L & S Band images using MGFF which is TIF. DWT represents contrast on images. The L and S band SAR fusion is better in DWT. But multimodal fusion in weighted average, the combination of MGFF and TIF working principle keep image features.

VI. CONCLUSION

Image fusion using the S-band and L-band NISAR pictures shown in our article utilising this method successfully incorporates data from both bands, outperforming pan-sharpening approaches and working quicker than other-based systems, This method has its inbuilt ability for co-registration. Also it was shown that the recommended strategy outperformed/performed comparably to other techniques in most situations when compared to quantitative criteria, and it outperformed other methods in terms of visual quality. Many satellite photography missions, such as Landsat and Sentinel, as well as SAR imagery of an area; such as Air SAR and UAVSAR data generate pictures from various sensors, which must frequently be fused to utilise a single image rather than multiple views. A powerful multichannel fusion approach for NISAR pictures is formed via an pixel based diffusion method. We performed a multilooking technique on AVIRIS data and got 1st channel for ore findings which was merged with geofolki coregistered data and diffused with the L & S-band. This is to broaden the scope of the suggested method's application, we additionally expand the formulation such that it may fuse picture pairings without pre-registration. Through numerical comparisons of several measures using 7 more cutting-edge fusion techniques, it is shown that our technique can not only pinpoint the most crucial data but may also maintain the most or nearly greatest quantity of data in the original photographs. This is also to be noted on ore finding using AVIRIS 54 number band. Hence we are preparing for drone settings in the near future. This work will produce the type of mine with the USGS spectral map hence it is very crucial work in the mining industry.

8. Algorithm 1 for ore Mining Type (Ashmit 2 Transform)

```
close all;clc;clear all;
% addpath(genpath('E:\'));
imgI=imread('a12.jpg');
data0=imgI;%imread('a.jpg');
data=data0;%(300:600,400:800,1:3);
figure,imagesc(data);
title('original image');
imgIR0=uint8(data);
var0=(double(imgIR0)-mean(imgIR0(:))).^2;
%
med=double(median(imgIR0(:)));
SNR0=mean(imgIR0(:)).*med ./ var0;
figure,imagesc(SNR0/255);   %Red band
title('water content');
%
%
% [out1, out2]=meshgrid(SNR0,1);
% out1=downsample(out1,1000)/1e5;
% out2=downsample(out2,1000)/1e5;
% out3=sqrt(out1.^2+out2.^2);
% figure,
%
% stem3(out1,out2,out3,'b');
%
% [R,G,B] = imsplit(SNR0);
% figure,imagesc(G>2e5 & G<3e5);
% title('green2')
cc1=rgb2cmyk1(imgIR0);
cc2=rgb2cmyk1(imgIR0);
figure,imagesc(squeeze(cc1(:,:,1)));   %Red band
figure,imagesc(squeeze(cc2(:,:,2)));   %Red band
figure,imagesc(squeeze(cc1(:,:,3)));   %Red band
figure,imagesc(squeeze(cc2(:,:,4)));   %Red band
```

9. Algorithm 2 for Radiative Mining Type (Ashmit 2 Transform)

```
close all;clc;clear all;
% addpath(genpath('E:\'));
imgI=imread('ab1.jpg');
data0=imgI;%imread('a.jpg');
data=data0;%(300:600,400:800,1:3);
figure,imagesc(data);
title('original image');
imgIR0=uint8(data);
var0=(double(imgIR0)-mean(imgIR0(:))).^2;
%
med=double(median(imgIR0(:)));
SNR0=mean(imgIR0(:)).*med ./ var0;
figure,imagesc(SNR0/255);   %Red band
title('water content')
```


ACKNOWLEDGEMENT

The authors are thankful to Ksitij Kumar Verma, Dr. Tapan Misra, Dr. Arundhati Misra, Dr. Avik Bhattacharya and Dr. Amitabha Bhattacharya and other teachers who have been very helpful.

DECLARATION STATEMENT

Funding	No, I did not receive.
Conflicts of Interest	No conflicts of interest to the best of our knowledge.
Ethical Approval and Consent to Participate	No, the article does not require ethical approval and consent to participate with evidence.
Availability of Data and Material	Not relevant.
Authors Contributions	All authors have equal participation in this article.

REFERENCES

1. M. Costantini et al., "Automatic Coregistration of SAR and Optical Images Exploiting Complementary Geometry and Mutual Information," IGARSS 2018 - 2018 IEEE International Geoscience and Remote Sensing Symposium, 2018, pp. 8877-8880, doi: 10.1109/IGARSS.2018.8519242.

https://doi.org/10.1109/IGARSS.2018.8519242

2. A. Plyer, E. Colin-Koeniguer and F. Weissgerber, "A New Coregistration Algorithm for Recent Applications on Urban SAR Images," in IEEE Geoscience and Remote Sensing Letters, vol. 12, no. 11,pp.2198-2202,Nov.2015,doi:10.1109/ LGRS.2015.2455071. https://doi.org/10.1109/LGRS.2015.2455071
3. Scheffler, Daniel & Hollstein, André & Diedrich, Hannes & Segl, Karl & Hostert, Patrick. (2017). AROSICS: An Automated and Robust Open-Source Image Co-Registration Software for Multi-Sensor Satellite Data. Remote Sensing. 2017. 676. 10.3390/rs9070676. https://doi.org/10.3390/rs9070676
4. M. Costantini et al., "Automatic Coregistration of SAR and Optical Images Exploiting Complementary Geometry and Mutual Information," IGARSS 2018 - 2018 IEEE International Geoscience and Remote Sensing Symposium, 2018, pp. 8877-8880, doi: 10.1109/IGARSS.2018.8519242. https://doi.org/10.1109/IGARSS.2018.8519242
5. D. P. Bavirisetti and R. Dhuli, "Fusion of Infrared and Visible Sensor Images Based on Anisotropic Diffusion and Karhunen-Loeve Transform," in IEEE Sensors Journal, vol. 16, no. 1, pp. 203-209, Jan.1, 2016, doi: 10.1109/JSEN.2015.2478655. https://doi.org/10.1109/JSEN.2015.2478655
6. B. K., Shreyamsha Kumar. (2015). Image fusion based on pixel significance using cross bilateral filter. Signal, Image and Video Processing. 9. 1193-1204. 10.1007/s11760-013-0556-9. https://doi.org/10.1007/s11760-013-0556-9
7. Liu, Yu & Chen, Xun & Cheng, Juan & Peng, Hu & Wang, Z.. (2017). Infrared and visible image fusion with convolutional neural networks. International Journal of Wavelets, Multiresolution and Information Processing. 16. 10.1142/S0219691318500182. https://doi.org/10.1142/S0219691318500182
8. Zhou, Zhiqiang & Dong, Mingjie & Xie, Xiaozhu & Gao, Zhifeng. (2016). Fusion of infrared and visible images for night-vision context enhancement (Code available in Linked data). Applied Optics. 55. 6480-6490. 10.1364/AO.55.006480. https://doi.org/10.1364/AO.55.006480
9. Civardi, Gaia Letizia & Bechini, Michele & Colombo, Alessandro & Quirino, Matteo & Piccinin, Margherita & Lavagna, Michelle. (2022). VIS-TIR Imaging for Uncooperative Objects Proximity Navigation: a Tool for Development and Testing.
10. Bavirisetti, Durga & Xiao, Gang & Zhao, Junhao & Dhuli, Ravindra & Liu, Gang. (2019). Multi-scale Guided Image and Video Fusion: A Fast and Efficient Approach. Circuits, Systems, and Signal Processing. 38. 10.1007/s00034-019-01131-z. https://doi.org/10.1007/s00034-019-01131-z
11. Durga Prasad Bavirisetti, Ravindra Dhuli,Two-scale image fusion of visible and infrared images using saliency detection,Infrared Physics & Technology,Volume 76,2016,Pages 52-64,ISSN 13504495,https://doi.org/10.1016/j.infrared.2016.01.009. https://doi.org/10.1016/j.infrared.2016.01.009
12. Ma, Jinlei & Zhou, Zhiqiang & Wang, Bo & Zong, Hua. (2017). Infrared and visible image fusion based on visual saliency map and weighted least square optimization (Code available in Linked data). Infrared Physics & Technology. 82. 10.1016/j.infrared.2017.02.005. https://doi.org/10.1016/j.infrared.2017.02.005
13. Z. Liu, E. Blasch, Z. Xue, J. Zhao, R. Laganiere, and W. Wu, "Objective assessment of multiresolution image fusion algorithms for context enhancement in night vision: A comparative study," IEEE Transactions on Pattern Analysis and Machine Intelligence, vol. 34, pp. 94–109, 2012. https://doi.org/10.1109/TPAMI.2011.109
14. X. Zhang, P. Ye and G. Xiao, "VIFB: A Visible and Infrared Image Fusion Benchmark," 2020 IEEE/CVF Conference on Computer Vision and Pattern Recognition Workshops (CVPRW), Seattle, WA, USA, 2020, pp. 468-478, doi: 10.1109/CVPRW50498.2020.00060. https://doi.org/10.1109/CVPRW50498.2020.00060
15. D. P. Bavirisetti, G. Xiao and G. Liu, "Multi-sensor image fusion based on fourth order partial differential equations," 2017 20th International Conference on Information Fusion (Fusion), 2017, pp. 1-9, doi: 10.23919/ICIF.2017.8009719. https://doi.org/10.23919/ICIF.2017.8009719
16. Zhou, Zhiqiang & Dong, Mingjie & Xie, Xiaozhu & Gao, Zhifeng. (2016). Fusion of infrared and visible images for night-vision context enhancement (Code available in Linked data). Applied Optics. 55. 6480-6490. 10.1364/AO.55.006480. https://doi.org/10.1364/AO.55.006480
17. Jiayi Ma, Chen Chen, Chang Li, Jun Huang,Infrared and visible image fusion via gradient transfer and total variation minimization,Information Fusion,2016.
18. Lloyd Haydn Hughes, Diego Marcos, Sylvain Lobry, Devis Tuia, Michael Schmitt," A deep learning framework for matching of SAR and optical imagery" ,ISPRS Journal of Photogrammetry and Remote Sensing, Volume 169, 2020, Pages 166-179, ISSN 0924-2716, https://doi.org/10.1016/j.isprsjprs.2020.09.012
19. Aritro Pal Choudhury, Tamesh Halder, Rintu Kumar Gayen, Arundhati Misra Ray, Debashish Chakravarty," C-band and L-band AirSAR image fusion technique using anisotropic diffusion", Materials Today: Proceedings, Volume 58, Part 1, 2022, Pages 433-436,10.1016/j.matpr.2022.02.393. https://doi.org/10.1016/j.matpr.2022.02.393
20. Pajares, Gonzalo & de la Cruz, Jesús. (2004). A wavelet-based image fusion tutorial. Pattern Recognition. 37. 1855-1872. 10.1016/j.patcog.2004.03.010. https://doi.org/10.1016/S0031-3203(04)00103-7
21. Ehlers, Manfred, Klonus, Sascha, Johan Åstrand, Pär;"Multi-sensor image fusion for pansharpening in remote sensing" International Journal of Image and Data Fusion 25-45Taylor & Francis 1947-9832 doi: 10.1080/19479830903561985 https://doi.org/10.1080/19479830903561985
22. M. Neumann, L. Ferro-Famil, and E. Pottier, "A general model-based polarimetric decom- position scheme for vegetated areas," in Proceedings of the 4th International Workshop on Science and Applications of SAR Polarimetry and Polarimetric Interferometry (ESRIN), Fras- cati, Italy, 26–30, Citeseer (2009).
23. Safy*, M., Eltanany, A. S., & Amein, A. S. (2019). SAR Images Co-registration Based on Gradient Descent Optimization. In International Journal of Innovative Technology and Exploring Engineering (Vol. 9, Issue 2, pp. 2361–2367). https://doi.org/10.35940/ijitee.b6226.129219
24. Abdel-Wahab*, A. M., Abdel-Gawad, A. K., & AWAD, A. A. D. I. (2020). Urban Expansion Classification using the Change Detection of High-Resolution Images, for Jeddah Province. In International Journal of Recent Technology and Engineering (IJRTE) (Vol. 8, Issue 6, pp. 5080–5092). https://doi.org/10.35940/ijrte.f9813.038620
25. Image Enhancement based on Fusion using 2D LPDCT and Modified PCA. (2019). In International Journal of Engineering and Advanced Technology (Vol. 8, Issue 6S3, pp. 1482–1492). https://doi.org/10.35940/ijeat.f1264.0986s319
26. Sharma, Dr. K., & Garg, N. (2021). An Extensive Review on Image Segmentation Techniques. In Indian Journal of Image Processing and Recognition (Vol. 1, Issue 2, pp. 1–5). https://doi.org/10.54105/ijipr.b1002.061221
27. Nasir, F. M., & Watabe, H. (2020). Validation of the Image Registration Technique from Functional Near Infrared Spectroscopy (fNIRS) Signal and Positron Emission Tomography (PET) Image. In International Journal of Management and Humanities (Vol. 4, Issue 9, pp. 63–69). https://doi.org/10.35940/ijmh.i0877.054920

AUTHORS PROFILE

Tamesh Halder, Department of Mining Engineering, Indian Institute of Technology, Kharagpur, India Publication Topics Unmanned Aerial Vehicles, Synthetic Aperture Radar, Ad Hoc Networks, Agroforestry, Digital Elevation Model, Extreme Learning Machine, Flying Ad Hoc Networks, Global Positioning System, Path Loss, Point Cloud, Point Cloud Model, Polarimetric Synthetic Aperture Radar, Receiver Operating Characteristic Curve,3D Mesh, Acid Mine Drainage, Acquisition Unit, Adaptive Algorithm, Adaptive Filter, Additive Noise, Aerial Images, Aerodynamic, Agisoft Photo Scan, Area Under Curve, Artifact Removal, Atmospheric Oxygen **Biography** Tamesh Halder received the B.Tech. degree in electronics and instrumentation engineering from the University of Kalyani in 2010, and the M.S. degree in electronics and electrical communications engineering from the Indian Institute of Technology Kharagpur, Kharagpur, in 2013, where he is currently pursuing the Ph.D. degree with the Department of Mining Engineering. His research experience includes remote sensing, focal source localization, compressive sensing, beamformers, receiver operating characteristics, EEG, MEG, and machine learning.

Published By:
Blue Eyes Intelligence Engineering
and Sciences Publication (BEIESP)

Dipanjan Dutta, Skills and expertise Image Analysis, Antenna Design, VLSI Design, Electronics and Communication Engineering He is pursuing 4th year BTech in KIIT University on School of Electronics (July 2020 to July 2024), He is also "Student Secretary" of "APS Society" and Vice Chair of IEEE Student Branch ,Member of Optic society, Member of MTT Society.

Abhishek Penchala, Abhishek Penchala is a research scholar at the Department of Mining Engineering, Indian Institute of Technology Kharagpur. His primary area of research includes the measurement and prediction of particulate matter (PM) in surface mines using low-cost sensor technology integrated with unmanned aerial vehicles (UAV). He obtained a bachelor's degree in Mining Engineering in the year 2017. He worked as a mining engineer at Hindustan Zinc Limited (HZL), Vedanta Plc, and holds a second-class mines manager certificate from the Director General of Mine Safety (DGMS). Air Quality Research Laboratory (AQRL), Department of Mining Engineering, Indian Institute of Technology Kharagpur, Kharagpur, India.

Vamshi Krishna Kandukuri, He worked as a mining engineer at Hindustan Zinc Limited (HZL), Vedanta Plc, Currently he is field engineer in Zewar Mines, Rajasthan, India. Where Zinc and Led is available but he did fieldtrip to Zinc area helping corresponding author.

Grajula Prashnath, He was employed by Vedanta Plc and Hindustan Zinc Limited (HZL) as a mining engineer. At the moment, he works as a field engineer at Zewar Mines in Rajasthan, India. Where Zinc and Led are accessible, but he assisted the corresponding author on a field trip to the Zinc area.

Debashish Chakravarty, Mining Engineering, Indian Institute of Technology Kharagpur Kharagpur, India Publication Topics Unmanned Aerial Vehicles,Global Positioning System,Synthetic Aperture Radar,Ad Hoc Networks,Agroforestry,Convolutional Neural Network,Digital Elevation Model,EEG Data,Extreme Learning Machine,Flying Ad Hoc Networks,Land Use,Land Use/land Cover,Machine Learning,Mining Regions,Normalized Difference Vegetation Index,Path Loss,Performance Metrics,Point Cloud,Point Cloud Model,Polarimetric Synthetic Aperture Radar,Receiver Operating Characteristic Curve,Water Bodies,3D Mesh,Acid Mine Drainage,Acquisition Unit Biography Debashish Chakravarty received the B.Tech. and M.Tech. degrees in mining engineering, the Ph.D. degree from the Indian Institute of Technology Kharagpur, Kharagpur, in 1998, and the Postdoctoral degree in applied mathematics and computer science from BAT, Germany, in 2003. He is an Associate Professor with the Department of Mining Engineering, Indian Institute of Technology Kharagpur. He is the Professor-in-Charge of the Autonomous Ground Vehicle Students' Research Group. He is also associated with the Advanced Technology Development Centre, Indian Institute of Technology Kharagpur. His areas of research are remote sensing, rock mechanics, numerical modelling, and geoinformatics.

Retrieval Number: 100.1/ijese.A805513010524
DOI: 10.35940/ijese.A8055.12060524
Journal Website: www.ijese.org

Published By:
Blue Eyes Intelligence Engineering
and Sciences Publication (BEIESP)